Article

Fluorination of Photoswitchable Muscarinic Agonists Tunes Receptor Pharmacology and Photochromic Properties

Luca Agnetta, Marcel Bermudez, Fabio Riefolo, CARLO MATERA, Enrique Claro, Regina Messerer, Timo Littmann, Gerhard Wolber, Ulrike Holzgrabe, and Michael Decker

J. Med. Chem., **Just Accepted Manuscript** • DOI: 10.1021/acs.jmedchem.8b01822 • Publication Date (Web): 03 Mar 2019

Fluorination of Photoswitchable Muscarinic Agonists Tunes Receptor Pharmacology and Photochromic Properties

Luca Agnetta[†], Marcel Bermudez[$], Fabio Riefolo[§#], Carlo Matera[§#], Enrique Claro[¥], Regina Messerer[†], Timo Littmann[‡], Gerhard Wolber[$], Ulrike Holzgrabe[†], Michael Decker[†*]

[†]Pharmaceutical and Medicinal Chemistry, Institute of Pharmacy and Food Chemistry, Julius Maximilian University of Würzburg, Am Hubland, 97074 Würzburg, Germany.

[s]Institute of Pharmacy, Freie Universität Berlin, Königin-Luise-Straße 2 + 4, 14195 Berlin, Germany.

§Institute for Bioengineering of Catalonia (IBEC), Barcelona Institute for Science and Technology, Carrer Baldiri Reixac 15-21, 08028 Barcelona, Spain.

[#]Network Biomedical Research Center in Bioengineering, Biomaterials, and Nanomedicine (CIBER-BBN), 50018 Zaragoza, Spain.

[¥]Institut de Neurociències (INc), and, Dept. Bioquímica i Biologia Molecular, Unitat de Bioquímica de Medicina, Universitat Autònoma de Barcelona (UAB), 08193 Bellaterra, Barcelona, Spain.

‡Institute of Pharmacy, University of Regensburg, Universitätstraße 31, 93053 Regensburg, Germany.

ABSTRACT: Red-shifted azobenzene scaffolds have emerged as useful molecular photoswitches to expand potential applications of photopharmacological tool compounds. As one of them, tetra-*ortho*-fluoro azobenzene is well compatible for the design of visible light responsive systems, providing stable and bidirectional photoconversions and tissue-compatible characteristics. Using the unsubstituted azobenzene core and its tetra-*ortho*-fluorinated analog we have developed a set of uni- and bivalent photoswitchable toolbox derivatives of the highly potent muscarinic acetylcholine receptor agonist iperoxo. We investigated the impact of the substitution pattern on receptor activity and evaluated the different binding modes. Compounds **9b** and **15b** show excellent photochemical properties and biological activity, as fluorination of the azobenzene core alters not only the photochromic behavior, but also the pharmacological profile at the muscarinic M_1 receptor. These findings demonstrate that incorporation of fluorinated azobenzenes may alter not just photophysical properties but can exhibit a considerably different biological profile that has to be carefully investigated.

INTRODUCTION

In recent years, many different biochemical targets, including ion channels, enzymes and lipids have been effectively modulated in a light-controlled fashion using photoswitchable ligands, expanding the vibrant field of photopharmacology.[1] Now, the potential of the application of photopharmacological tool compounds to G protein-coupled receptors (GPCRs) is being steadily investigated.[2] The rapid light-induced isomerization of photochromic ligands can be directly translated into a change in affinity or activity. This can give important new insights into binding mode and time course of activation processes enabling precise spatial and temporal resolution of the complex signaling pathway of GPCRs.[3] The muscarinic acetylcholine receptors (mAChRs), which belong to class A GPCRs, have received special attention in this regard, due to their role as prototypic pharmacological system[4] and their therapeutic potential.[5] The muscarinic receptors mediate the excitatory and inhibitory effects of the neurotransmitter acetylcholine (ACh)[6] thus regulating diverse important biological processes. Muscarinic receptors are widely expressed in the human body including the central nervous system ($M_1/M_4/M_5$) related to neurological processes of memory and learning. In the peripheral nervous system (M_2/M_3) they are related to the so-called "rest and digest"

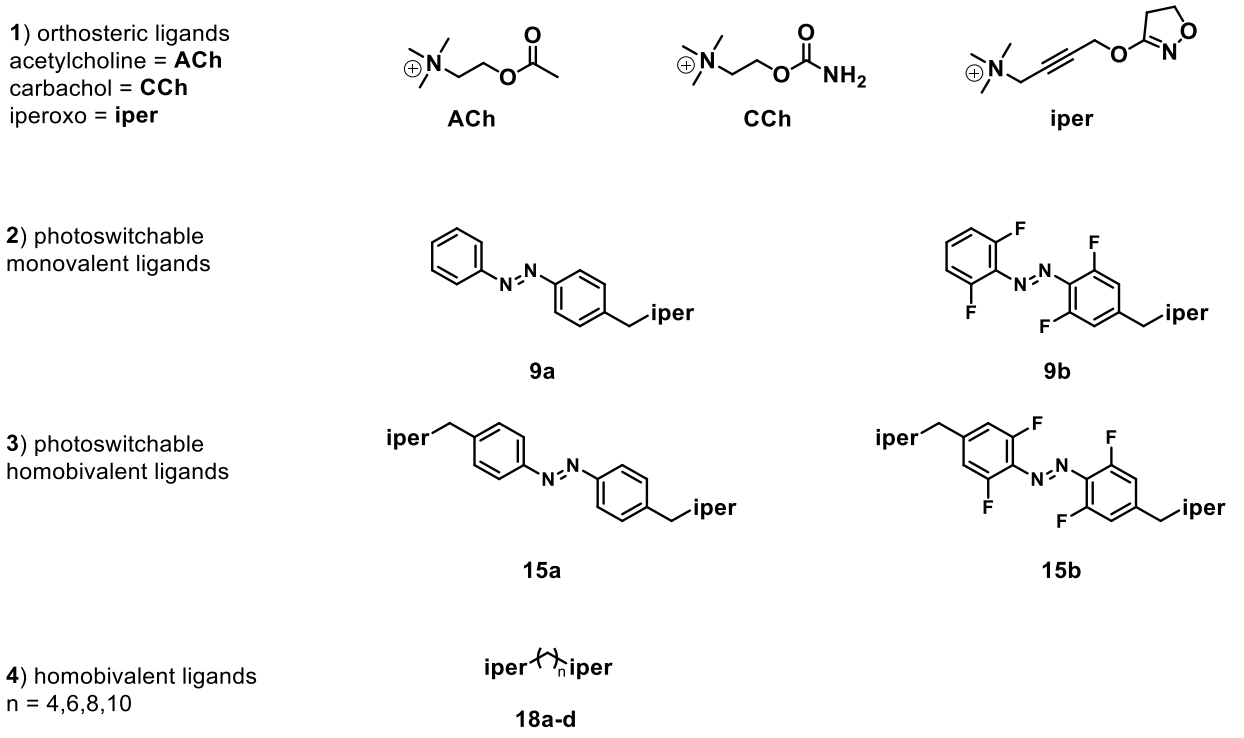

Figure 1. Structures of 1) reference agonists acetylcholine (ACh), carbachol (CCh) and iperoxo (iper) 2) univalent, 3) homobivalent photoswitchable derivatives with azobenzene- and tetra-*ortho*-fluoro azobenzene scaffolds and homobivalent ligands linked by polymethylene linkers.

biological functions.[7] In this work we present an optimized approach for the application of photochromic ligands to GPCRs by using the M_1 receptor as a prototypic model system, outlining the advantages and challenges of using redshifted molecular photoswitches.

Accordingly, we focused on the highly potent orthosteric agonist iperoxo in the design of bidirectional pharmacological tool compounds with tuned photochemical properties. Iperoxo is a muscarinic ACh receptor agonist with outstanding potency that is known to tolerate bulky substituents without compromising agonist efficacy.[8] Recently, we reported on photoiperoxo (**9a**), a compound that consists of iperoxo extended with a molecular photoswitch and a dualsteric photochromic ligand **BQCAAI.**[2c] We made use of azobenzene as a molecular photoswitch to change intrinsically the geometry and polarity of the linking unit and to control its activation by light.[1a, 1b, 1d] Upon irradiation with UV- and blue light, and thus triggering a switch from the *trans*- to the *cis*-form, we were able to control the efficacy and to investigate the time course of receptor activation processes.[2c]

Scheme 1. Synthesis of photoiperoxo and F_4-photoiperoxo[a]

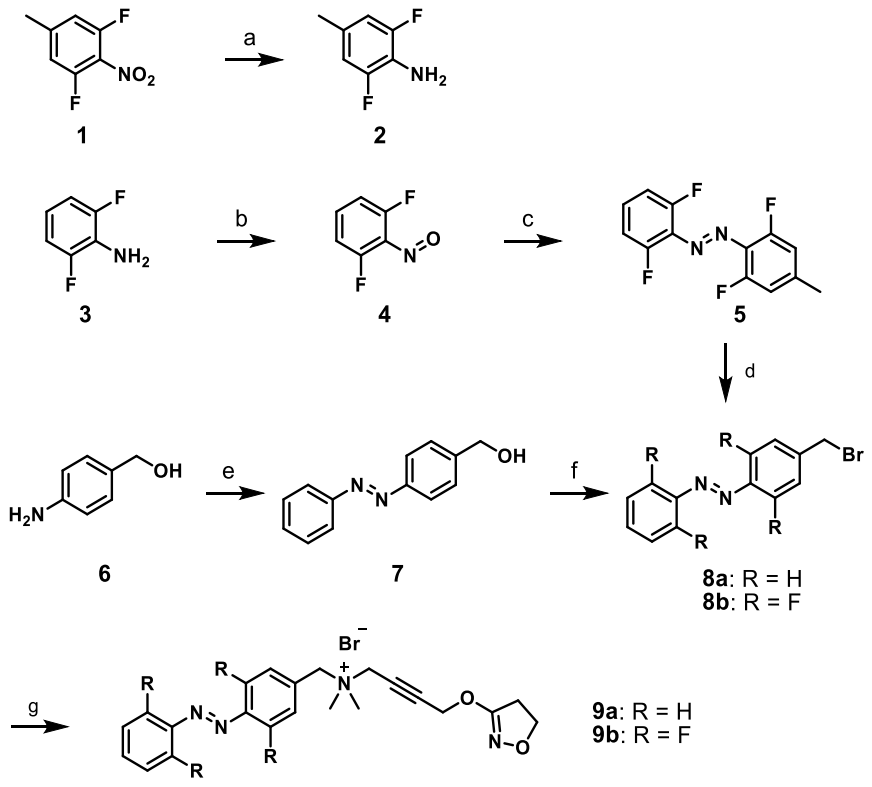

[a]Reagents and conditions: (a) Pd/C, EtOH (87%); (b) Oxone, CH_2Cl_2, water; (c) **2**, AcOH/TFA, toluene (43%); (d) NBS, AIBN, CCl_4, 80 °C (50%); (e) nitrosobenzene, AcOH (75%); (f) CBr_4, PPh_3, CH_2Cl_2 (60%); (g) 4((4,5-Dihydroisoxazol-3-yl)oxy)-*N*,*N*-dimethylbut-2-yn-1-amine **16**, EtOAc/MeCN (39% for **9a**, 92% for **9b**).

Scheme 2. Synthesis of iper-azo-iper and F_4-iper-azo-iper[b]

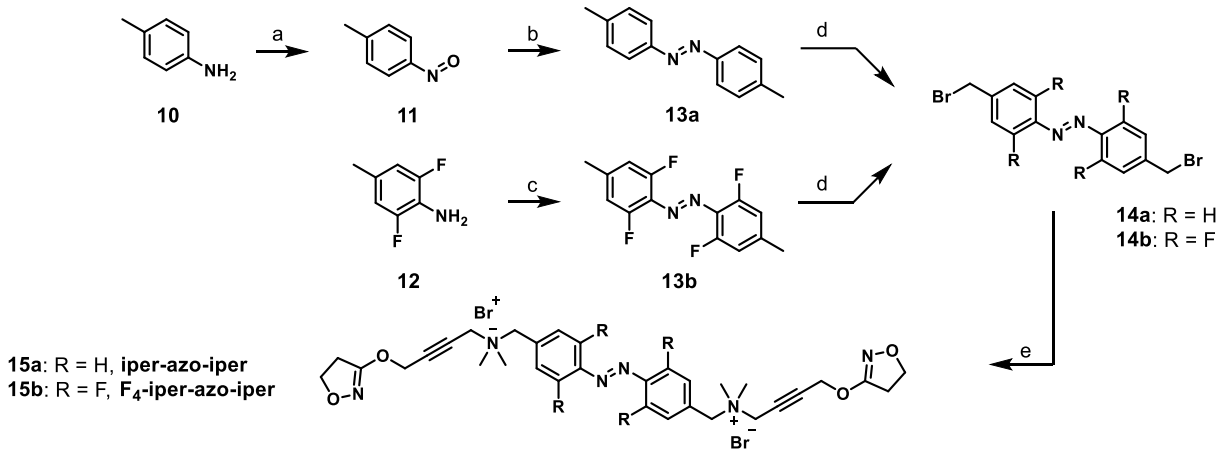

[b]Reagents and conditions: (a) Oxone, CH_2Cl_2, water; (b) **10**, AcOH (36%); (c) $KMnO_4$, $FeSO_4{\cdot}7H_2O$, CH_2Cl_2 (29%); (d) NBS, AIBN, CCl_4, 80 °C (76% for **14a**, 24% for **14b**); (e) 4((4,5-Dihydroisoxazol-3-yl)oxy)-*N*,*N*-dimethylbut-2-yn-1-amine, EtOAc, 60 °C (83% for **15a**, 32% for **15b**).

Despite this remarkable progress in the development of photopharmacological tool compounds, the poor photostationary states (PSSs) of our azobenzene-based systems resulted in an unclear correlation between the ratio of the *cis*/*trans* concentration to the actual activity at the receptor. The PSS strongly depends on the electronic environment of the system and the overlap of transitions of the c*is/trans* photoisomers and can be influenced by changing the substitution pattern of the azobenzene moiety. Additionally, the operational wavelengths to trigger photoisomerization can interfere to a significant degree with the fluorescent readout methods that are commonly used in GPCR research. To investigate the complex nature of M_1 activation, photopharmacological tool compounds should ideally show superior photochemical properties, such as quantitative and stable bidirectional photoswitching and be responsive to visible rather than high energy light.[1a, 1b, 1d] A convincing approach to optimize the photochemical properties of azobenzenes involving the tetra-*ortho*-substitution of azobenzene has been described previously by the groups of Woolley[9] and Hecht.[10] By choosing the suitable moieties, tetra-*ortho*-substitution leads to a separation of the n→π* transitions of *trans* and *cis* isomers and ultimately to almost complete *trans*/*cis* photoconversions. Importantly, the desired isomer can be selectively formed with wavelengths in the visible light window. Despite their promising application in photobiology due to the well separated n→π* transitions,[11] *ortho*-methoxylated azobenzenes are sterically demanding and strongly twisted about the N-N double bond. This makes them unlikely to fit into the narrow receptor binding pocket. *Ortho*-chlorinated and fluorinated azobenzenes show comparable red-shifted *trans*

n-π* transitions, albeit somewhat less than *ortho*-methoxylated and have been successfully employed in biological applications.[12] However, tetra-*ortho*-fluoro substituted azobenzenes stand out in their slow thermal *cis*-to-*trans* relaxation rate, representing a truly bistable molecular switch on biological time scale. Moreover, the fluorine substituents are sterically less demanding compared to the chlorine ones.[10a] Based on these results we further investigated the effect of iperoxo-derived photoswitchable ligands by developing a set of tool compounds, containing the iperoxo motif and the tetra-*ortho*-fluoro azobenzene or unsubstituted azobenzene, respectively.

In modern medicinal chemistry, the bivalent strategy has been extensively applied to GPCR ligands.[13] Appropriately designed bivalent ligands can exhibit higher affinity, potency and selectivity compared with the parent ligand, with potential therapeutic application.[14] Successful examples of the application of this approach to GPCRs include the human cannabinoid receptor 2 (*h*CB2),[15] opioid receptor (OR),[16] dopamine 2 (D2)[17] and muscarinic receptors.[18] To this end, we extended the photoiperoxo structure with another iperoxo moiety, creating a homobivalent ligand, to improve and investigate binding at the M_1 receptor.

RESULTS AND DISCUSSION

We now report the design and synthesis of photoswitchable homobivalent iperoxo (**15a**), tetra-*ortho*-fluoro-photoiperoxo (**9b**) and homobivalent tetra-*ortho*-fluoro-photoiperoxo (**15b**), being the corresponding tetra-*ortho*-fluorinated analogs of the azobenzene iperoxo derivatives (**Figure 1**). In addition, we synthesized homobivalent iperoxo derivatives (**18a-d**) connected by aliphatic chains as reference compounds to identify the optimal distance between the two orthosteric moieties for dualsteric binding.

Chemistry. The synthetic routes for the uni- and homobivalent ligands are summarized in **Schemes 1** and **2,** respectively. Azobenzene moieties **5** and **7** were accessed starting from the corresponding anilines **2**, obtained from reduction of 1,3-difluoro-5-methyl-2-nitrobenzene **1,** and commercially available (4-aminophenyl)methanol **6**. Anilines were used in Baeyer-Mills reactions with 1,3-difluoro-2-nitrosobenzene **4** and nitrosobenzene, respectively, to afford precursors for bromination, which took place either under radical (for **8b**) or nucleophilic substitution conditions (for **8a**). Lastly, 4((4,5-dihydroisoxazol-3-yl)oxy)-*N*,*N*-dimethylbut-2-yn-1-amine, prepared using the standard convergent procedure as described previously[19], was connected to the photoswitches to afford photoiperoxo **9a** and F_4-photoiperoxo **9b**.

The synthesis of the homobivalent ligands started from commercially available *p*-toluidine **10**, which was condensed to compound **13a** by means of a Baeyer-Mills reaction. Tetra-*ortho*-fluorinated analogue **13b** was obtained by oxidative coupling of **12** with potassium permanganate and iron sulfate heptahydrate as oxidizing reagents. Again,

radical bromination and substitution with 4((4,5-dihydroisoxazol-3-yl)oxy)-*N*,*N*-dimethylbut-2-yn-1-amine resulted in formation of target compounds **15a** and **15b**. Aliphatic derivatives (**18a-d**) were synthesized reacting the corresponding double brominated aliphatic chains with two equivalents of 4((4,5-dihydroisoxazol-3-yl)oxy)-*N*,*N*-dimethylbut-2-yn-1-amine (**Suppl. Scheme 5**).

UV/Vis Spectroscopic Characterization. The UV/Vis absorption spectra of the set of compounds **9a,b** and **15a,b** were measured at a concentration of 50 μM in DMSO. For compounds **9a** and **15a** (with unsubstituted azobenzene scaffold), we observed a strong π-π* transition band at short wavelength ($\lambda_{\pi-\pi^*} \approx 320$ nm) and a weaker n-π* ($\lambda_{n-\pi^*} \approx 422$ nm) upon irradiation with blue light (400 nm, *trans* isomer). Irradiation with UV light (365 nm), and thus photoconversion to the *cis* isomer, leads to a decrease in absorbance intensity of the π-π* and increase of n-π* band

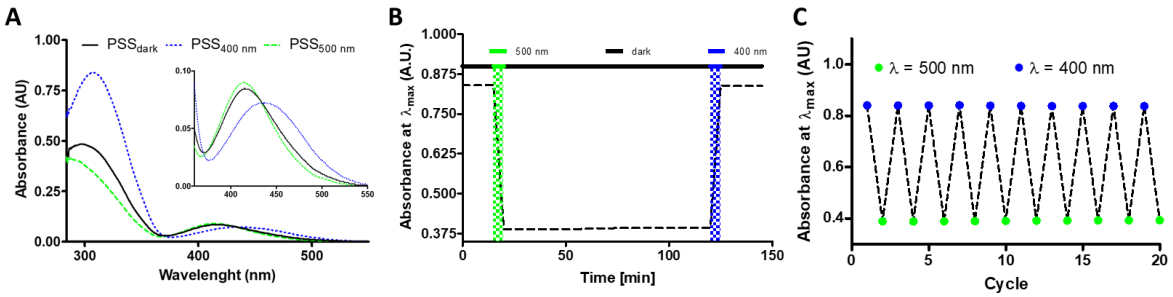

Figure 2. Representative (A) absorption spectra of PSS at the dark-adapted state and after illumination with 400 nm (to *trans*) and 500 nm (to *cis*), (B) stability measurement and (C) multiple *cis*/*trans* isomerization cycles of compound **9b** in dimethyl sulfoxide at 25°C. Spectra of compound **9a** and **15a,b** are displayed in Supplementary Information section.

Table 1. UV/VisSpectroscopic data of compounds 9a,b and 15a,b.[c]

Cmpd.	λ_{max} (π–π*)	ε (π–π*)	λ_{max} (n–π*)	ε (n–π*)	λ_{max} (n–π*)	ε (n–π*)	Δλ (n-π*)	PSS_{trans}	PSS_{cis}
	[nm]	*10³ [1/(M*cm)]	[nm]	[1/(M*cm)]	[nm]	*10³ [1/(M*cm)]	[nm]	%	%
	trans		trans		cis				
9a	320	12.2	418	680	418	1.04	<10	90	62
15a	320	22.0	426	920	426	1.42	<10	99	60
9b	307	16.7	443	1440	412	1.80	31	94	86
15b	311	14.8	447	1180	412	1.38	35	93	98

[c] λ_{max} (π–π*, n–π*) represents the wavelength at the maximal absorption of the π–π* and n–π* transition band, respectively. The molar extinction coefficient ε (π–π*, n–π*) were calculated according to Lambert-Beer. Δλ (n–π*) is the difference between *trans* and *cis* regarding λmax of n–π* band. PSS percentages after irradiation with operational wavelengths determined by liquid chromatography using the wavelength at the isosbestic point as detecting wavelength.

without affecting the wavelengths of the respective transition bands. Spectra of fluorinated compounds **9b** and **15b** were measured using 400 nm for *cis*→*trans* and 500 nm for *trans*→*cis* photoconversions. Due to the n-orbital stabilization of electron-withdrawing groups in the *cis*-state, tetra-*ortho*-fluoro substitution of the azobenzene core causes a separation of the transitions of the n-π* band, in our case of around 33 nm on average, which makes it possible to address both isomers selectively with light in the visible region (**Figure 1A**).[20] As a direct consequence, the PSSs (measured by means of liquid chromatography at the isosbestic point wavelength) are substantially higher than for non-fluorinated analogues (**Table 1**), which is beneficial for the application of photoswitchable ligands in biological systems and allows a clear correlation between the distinct photoisomer and its biological effect. Moreover, multiple *cis*/*trans* switching cycles did not cause noticeable degradation, highlighting the reliability and robustness of the photochromic conversion of both the tetra-*ortho*-fluoro and unsubstituted azobenzene scaffolds. This is confirmed by stability measurements in which the compounds were kept in the dark for at least 120 minutes after

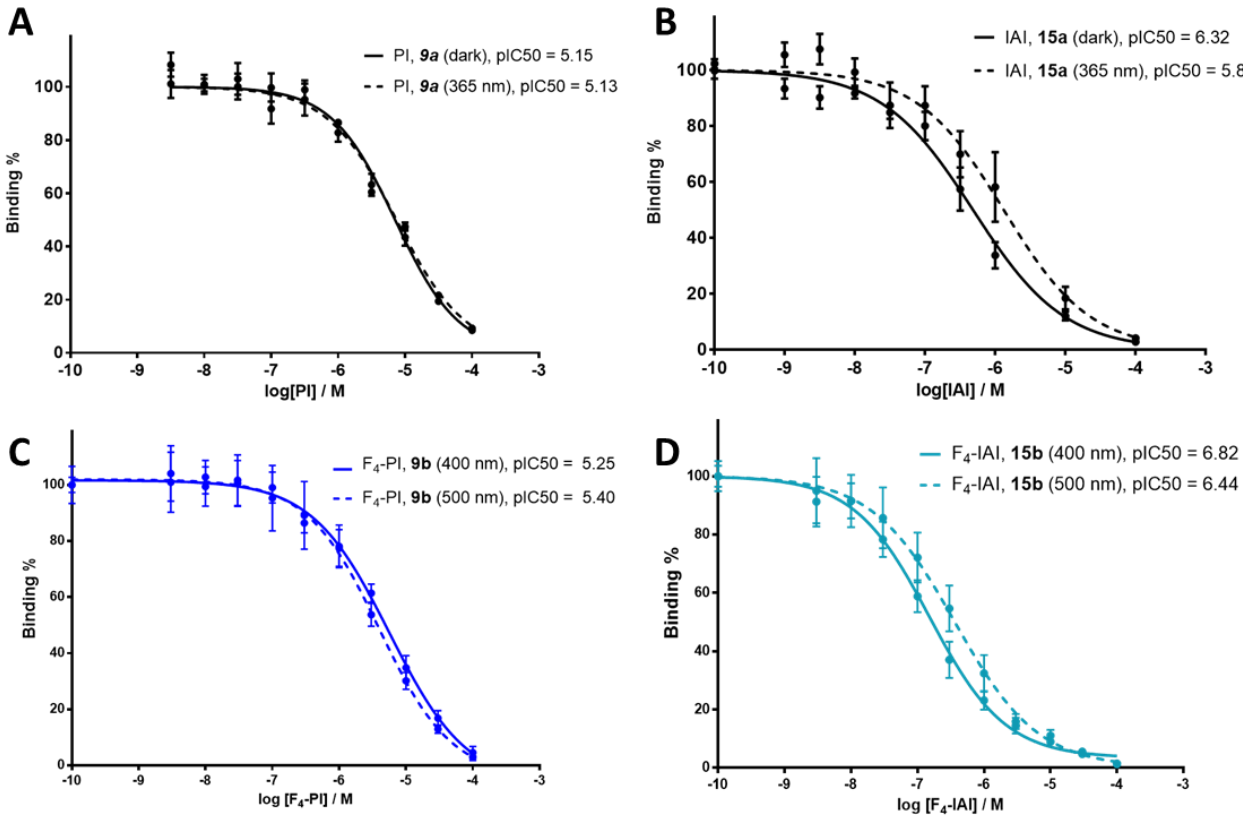

Figure 3. Competition for specific binding of 200 pM [3H]QNB to rat brain membranes containing high density of all the five mAChRs by **9a,b** and **15a,b**. Data points were fitted using the "log(inhibitor) vs. normalized response - Variable slope" function in GraphPad Prism 6.

switching to the less stable *cis*-isomer, without significant changes in absorbance and hence in the PSS. Importantly, this information is required when considering eventual incubation times required in biological assays, making sure that the photoswitchable ligands do not relax to the *trans*-isoform during the readout (**Figure 1B/C**). From the physicochemical point of view, this set of compounds shows ideal characteristics for stable and bidirectional photoswitching.

Binding experiments. Firstly, **9a,b** and **15a,b** were tested for affinity to the M receptors. This was achieved in competition experiments with the photoswitchable ligands in rat brain membrane preparations. These were conducted as described previously,[21] and contained a high density of all the five mAChR subtypes. [^{3}H]Quinuclidinyl benzilate ([^{3}H]QNB) is a nonselective muscarinic ligand, which allows the identification of muscarinic receptors[22], and displays an equilibrium dissociation constant of about 40 pM,[23] making it suitable for these experiments. Specific binding was defined with test compounds at total nominal concentrations in the range of 1 to 100 μM and elaborating the raw dpm data from the scintillation counter,[21] representing total radioactivity.

In general, the compounds **9a,b** and **15a,b** were found to show good affinity for the M receptors (**Figure 3**). In particular, the azobenzene-elongated iperoxo **9a** and **9b** showed a binding affinity in the low-micromolar range, although no significant changes could be observed upon irradiation (pIC50 ≃ 5 for both photoisomers, **Figure 3A/C**). The affinity increased significantly for the homobivalent ligand **15a** and **15b**. In good agreement with results from split-luciferase interaction assay, *trans*-**15a** showed an affinity in the high-nanomolar range, with a significant difference between the two photo isoforms (pIC50 = 6.32 in the dark versus 5.88 under illumination with 365 nm light, **Figure 3B**). Thus, we observed that despite the introduction of an azobenzene molecular photoswitch, a good affinity could be preserved. Moreover, the presence of a second moiety of iperoxo, as in the homobivalent ligand **15a** and **15b**, improved binding affinity and created an appreciable difference between *trans* and *cis* isomers.

Biological *in vitro* assay. Our goal was to assess the extent to which the pharmacological profiles of these compounds change after fluoro-substitution of the azobenzene core. For this purpose, we used a novel split luciferase complementation technique detecting the interaction between Gαq subunit and phospholipase C-β3 (PLC-β3) and thus reflecting G protein activation in living HEK 293T cells expressing the human M_1 receptor.[24] The split luciferase complementation technique is particularly suitable to detect protein-protein interactions and associated signaling in living cells.[25] Since it is not fluorescence-based, no excitement irradiation is needed and consequently, its readout does not interfere with the operational wavelengths for photoswitching, providing clear-cut and distinguishable

concentration-response-curves for each photoisomer, which makes it highly suitable for photo-pharmacological investigations into GPCRs. Technically, HEK 293T cells were engineered to express a fragment of the luciferase at the Gαq subunit of the heterotrimeric G protein and the complementary fragment at the *N*-terminus of the PLC- β3. Upon binding of the endogenous or synthetic agonists, both fragments are brought in close proximity leading to a reconstitution of the functional luciferase protein and emission of bioluminescence, in the presence of the substrate luciferin.[24] Also advantageous is the fact that the receptor itself, in this case M_1, remains un-engineered in contrast to e.g. FRET-sensors, where often large constructs at intracellular loops could act as anchors and may affect changes in conformations. Pharmacological data are depicted in **Figure 4** and summarized in **Table 2,** and show the recorded potencies and efficacies of compounds **9a,b** and **15a,b**, reflected by the pEC_{50}, and maximal response E_{max} for each isomer. The data are normalized to the maximum response of the synthetic agonist carbachol (CCh) at a concentration of 100 μM. Measurements of the endogenous agonists acetylcholine (ACh) and the synthetic parent compound iperoxo as references were not affected by illumination with operational wavelengths.

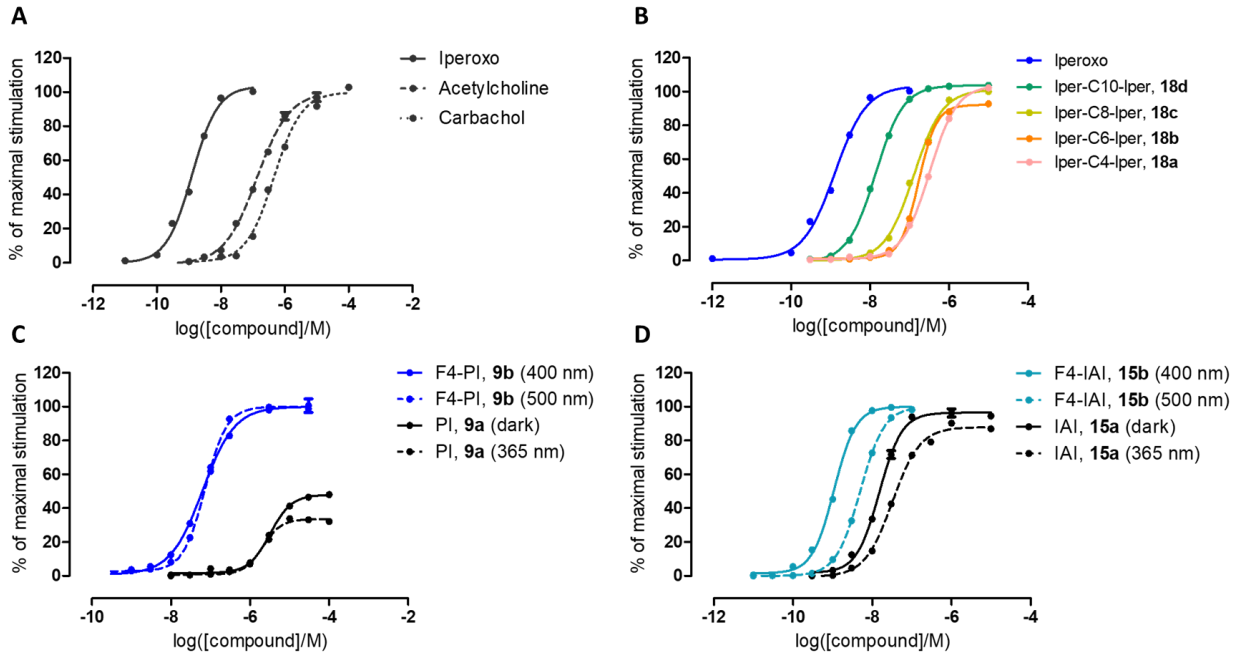

Figure 4. Gα/PLC-β3 split-luciferase interaction assay in HEK 293T cells expressing the human muscarinic M_1 receptors (hM_1). Concentration-response-curves for A) Reference compounds, B) Iper-linker-Iper derivatives (**18a-d**), C) **9a** and **9b** and D) **15a** and **15b** at operational wavelength specific for the respective photoconversion. Data represent means ± SEM of 3-4 experiments conducted at least in triplicate.

Firstly, bivalent alkyl-substituted iperoxo compounds were screened to identify the correlation between the distance of the orthosteric moieties and its corresponding biological activity. For this purpose, homobivalent ligands **18a-d** with different chain lengths were employed. All compounds were characterized as full agonists and longer spacer proved advantageous for M_1 affinity suggesting a dualsteric binding.[26] The C10-spacer, which is comparable to the azobenzene scaffold, shows the highest effect and suggests this distance as optimal for the design of photoswitchable ligands (**Suppl. Figure 1**).

As investigated in previous studies, photoiperoxo **9a** was unable to induce a conformational change at the M_1 receptor in FRET studies, neither upon illumination with UV- nor blue light. Instead, it exhibited antagonist behavior in competition experiments.[2c] Using the split luciferase complementation assay, **9a** shows two distinct curves for each photoisomer, differing in their efficacy. The maximal response E_{max} was 48% for the *trans* and 34% for the *cis* photoisomer, indicating partial agonism at the M_1 receptor. Surprisingly, substitution of azobenzene with the tetra-*ortho*-fluorinated scaffold resulted in full agonist **9b** with a significant potency enhancement and pEC_{50}-values almost two log units higher (comparable to endogenous agonist ACh). However, no significant changes in efficacy or affinity could be observed for **9b** upon irradiation.

The potency at the M_1 receptor was modulated effectively by introducing an additional iperoxo moiety resulting in the homobivalent ligand **15a**. By doing so, considerable improvement in the potency was gained and a difference between the two photoisomers was re-established. Again, replacement of the azo-core with tetra-*ortho*-fluoro

Table 2. Pharmacological data[d]

Cmpd.	*pEC_{50}*		*$\%E_{max}$*	
Iperoxo	8.90 ± 0.02		103.5 ± 1.0	
CCh	6.34 ± 0.02		99.9 ± 0.9	
ACh	6.87 ± 0.03		99.9 ± 1.8	
18a	6.49 ± 0.01		103.6 ± 0.6	
18b	6.77 ± 0.01		92.2 ± 0.6	
18c	6.89 ± 0.01		101.1 ± 0.8	
18d	7.86 ± 0.02		103.7 ± 0.7	
	trans	*cis*	*trans*	*cis*
9a	5.49 ± 0.01	5.68 ± 0.02	48.0 ± 0.4	33.5 ± 0.5
9b	7.20 ± 0.02	7.14 ± 0.01	98.3 ± 1.2	99.7 ± 0.6
15a	7.82 ± 0.02	7.49 ± 0.02	96.5 ± 1.1	87.9 ± 0.7
15b	8.97 ± 0.01	8.30 ± 0.02	99.7 ± 0.3	99.1 ± 0.4

[d]pEC_{50}, concentration of the indicated compounds inducing a half-maximal effect (–log EC50 values); $\%E_{max}$, maximum effect as a percentage of E_{CCh} (100 µM); Data were obtained by curve fitting to data from individual experiments shown in **Figure 4**.

scaffold (**15b**) resulted in a distinctive change toward higher potency, being almost 10-fold more pronounced for the *trans* isomer. Noteworthy, *trans*-**15b** shows a pEC_{50} concentration in the one-digit nanomolar range, which is comparable to the agonist iperoxo itself. This is a remarkable observation, as the introduction of a molecular photoswitch generally causes an overall loss in activity at the receptor. A photoswitch-endowed compound showing an almost identical potency as the reference compound is hard to achieve. Taken together, these findings suggest, that binding of *trans*-form of bivalent derivatives **15a**, **15b** and **9b** stabilizes the M_1 receptor in the active conformation to a greater extent than **9a**. Additionally, fluoro substitution leads to pronounced differences in biological activity and is beneficial for binding to the M_1 receptor. As such, we developed a set of photopharmacological GPCR tool compounds for a better understanding of M_1 receptor binding modes.

Molecular Modelling. Docking studies using a previously reported homology model of the active M_1 receptor conformation[27] reveal a dualsteric (bitopic) binding mode for all investigated photoswitchable iperoxo derivatives in their *trans* conformation (**Figure 5**). We surmise that the photoswitch primarily occurs in solution and that the pharmacological properties are mainly driven by binding of *trans* isomers. The active M_1 receptor model indicates a narrow channel between the orthosteric and the allosteric binding sites rendering binding of *cis* conformations to the receptor unlikely due to steric interference with the tyrosine lid. Similar to other iperoxo-based dualsteric ligands[28]

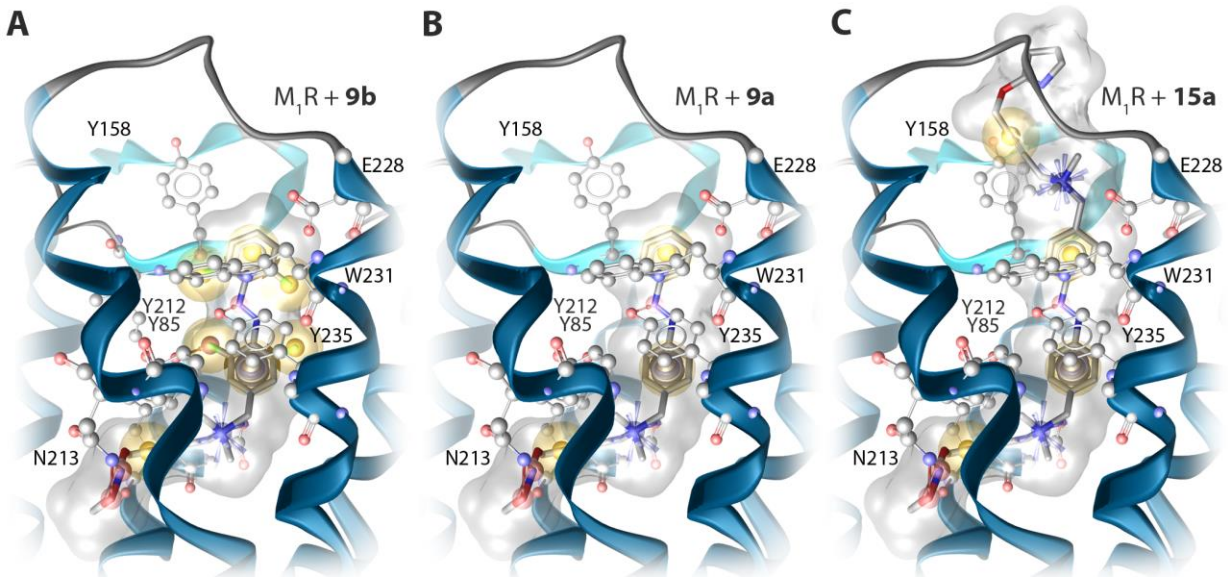

Figure 5. Proposed binding modes and interactions of *trans* isomers of photoswitchable dualsteric iperoxo derivatives (A) **9b**, (B) **9a** and (C) **15a** in complex with the M_1 receptor. Positive ionizable centres are shown as blue stars, yellow spheres indicate lipophilic contacts, purple disks show aromatic interactions and red arrows indicate hydrogen bonds.

the iperoxo moiety is located in the orthosteric binding pocket showing interactions with D84, N213 and the tyrosine lid consisting of Y85, Y212 and Y235 (**Figure 5**). For all compounds, a hydrogen bond between the azo group and the hydroxy group of Y235 is formed. The sidechain of Y235 shows a reorientation towards the extracellular side, which allows binding of azobenzene scaffolds through π-π interactions. This sidechain position allows full contraction of the orthosteric binding site without full closure of the tyrosine lid and thereby stabilizes active receptor conformations.

Interestingly, fluorination of the azobenzene scaffold results in a higher potency of **9b** and **15b** compared to the non-fluorinated compounds **9a** and **15a**. This can be rationalized in our model by an optimal geometry of the aromatic ring in the M_1 receptor. Whereas the phenyl ring opposite to Y235 is more flexible in **9a** and **15a**, it is restrained in an orientation, optimal for parallel π-π interaction. This is caused by the spatial requirements of the *ortho*-fluorine atoms in **9b** and **15b** and an additional hydrogen bond with the hydroxy group of Y85 (**Figure 5A**). In addition, fluorinated compounds show additional lipophilic contacts with the tyrosine lid as well as W231 (**Figure 5A/B**). Since the symmetric compounds **15a** and **15b** are larger, they show secondary interactions in the extracellular vestibule compared to **9a** and **9b**. In particular, a charge interaction of the ammonium group in the extracellular receptor domain with E228 can be observed (**Figure 5C**). Positive charges in the allosteric vestibule recognized by aromatic residues or the EDGE sequence have previously been found to be important for the M_2 receptor.[28b, 29]

Interestingly, the M_2 receptor lacks the presence of an acidic residue at the beginning of transmembrane domain 7, suggesting a specific role for E228 in the M_1 receptor. This observation is in accordance with the higher potencies for **15a** and **15b** that can be explained by this specific charge interaction and additional lipophilic contacts with Y158, which were not observed for **9a** and **9b** due to the lack of an allosteric ammonium group (**Figure 5**). The absence of extensive allosteric interactions and less lipophilic contacts of **9a** compared **9b** suggest a ligand-receptor complex in which **9a** is not able to fully stabilize the active receptor state. This is supported by previously reported FRET-based measurements indicating the insensitivity of the M_1 receptor upon **9a** binding with regard to conformational changes.[2c] However, the here applied Gα/PLC-β3 split-luciferase interaction assay unveiled **9a** as a weak partial agonist (E_{max} 34-48 %).

At first sight, it may appear conflicting that the *cis* photoisomers bind to the receptor and induce a receptor response, while the docking data predict only the *trans* photoisomers to bind. On a closer look, even though the fluorinated azobenzene scaffold provides higher PSS, a distinct percentage of *trans* isomer remains (**Table 1**), which can still bind and activate the receptor. On a logarithmic scale, as used for the binding and functional studies, even a small *trans* percentage shows a pronounced effect. An alternative explanation can be rationalized by a second purely allosteric

binding mode as shown for several other dualsteric ligands.[26, 28a] For such a binding pose the *cis* orientation is compulsory, forming π-π and cation-π interactions, which can, to a certain extent, favor the active state of the receptor. In contrast, the linear nature of the *trans* photoisomer is not suitable to solely bind to the allosteric binding site. At this stage, this is still subject of future investigations though.

CONCLUSION

We successfully developed a set of photopharmacological tools that allowed detailed investigation of the distinct effects of fluorination and bivalency on binding properties at the M_1 receptor. We designed photoswitchable iperoxo (**9a**) and bivalent iperoxo compounds (**15a**), as well as the redshifted congeners (**9b, 15b**) by introduction of tetra-*ortho*-fluoro scaffold. Bivalent compounds (**15a,b**) show much higher affinity compared to the univalent compounds (**9a,b**) due to additional interactions at allosteric binding sites. Remarkably, the fluorine compounds (**9b, 15b**) not only show improved operational wavelengths as shown in a novel, light-independent luciferase complementation assay, but also increased potency at the M_1 receptor. Bivalent and fluorinated photoiperoxo (**15b**) act as a pronounced affinity switches, while the univalent photoiperoxo acts as efficacy switch (**9a**). The work significantly enlarges the photopharmacological toolbox for mAChRs. We strongly recommend detailed pharmacological evaluation for redshifted compounds since their biological properties might differ significantly from the parent compound. It will be interesting to investigate the potential for *in vivo* photopharmacological control of this series.

EXPERIMENTAL SECTION

General Information. Common reagents and solvents were obtained from commercial suppliers (Aldrich, Steinheim, Germany; Merck, Darmstadt, Germany) and were used without any further purification. Tetrahydrofuran (THF) was distilled from sodium/benzophenone under an argon atmosphere. Microwave assisted reactions were carried out on a MLS-rotaPREP instrument (Milestone, Leutkirch, Germany) using 8-10 weflon disks. Melting points were determined on a Stuart melting point apparatus SMP3 (Bibby Scientific, UK). Thin-layer chromatography (TLC) was performed on silica gel 60 F254 plates (Macherey-Nagel, Düren, Germany) and spots were detected under UV light (λ=254 nm) or by staining with iodine. Merck silica gel 60 (Merck, Darmstadt, Germany) was used for chromatography (230-400 mesh) columns or performed on an Interchim Puri Flash 430 (Ultra Performance Flash Purification) instrument (Montluçon, France). Used columns are: Silica 25 g – 30 µm, Alox-B 40 g – 32/63 µm, Alox-B 25 g – 32/63 µm (Interchim, Montluçon, France). Nuclear magnetic resonance spectra were performed with a Bruker AV-400 NMR instrument (Bruker, Karlsruhe, Germany) in [d_6]DMSO, CDCl3, $(CD3)_2CO$. As internal standard, the signals of the deuterated solvents were used (DMSO-d6: ^1H 2.50 ppm, ^{13}C 39.52 ppm; CDCl3: ^1H 7.26 ppm, ^{13}C 77.16 ppm; (CD3)2CO: ^1H 2.05 ppm, ^{13}C 39.52 ppm). Abbreviation for data quoted are:

s, singlet; d, doublet; t, triplet; q, quartet; m, multiplet; br, broad; dd, doublet of doublets; dt, doublet of triplets; tt, triplet of triplets; tq, triplet of quartets. Coupling constants (J) are given in Hz. For purity and reaction monitoring, analytical HPLC analysis was performed with a system from Shimadzu equipped with a DGU-20A3R controller, LC20AB liquid chromatograph, and a SPD-20A UV/Vis detector. Stationary phase was a Synergi 4 µm fusion-RP (150×4.6 mm) column (Phenomenex, Aschaffenburg, Germany). Mobile phase a gradient of MeOH/water with 0.1% formic acid was used. Parameters: A = water, B = MeOH, V(B)/(V(A) + V(B)) = from 5% to 90% over 10 min, V(B)/(V(A) + V(B)) = 90% for 5 min, V(B)/(V(A) + V(B)) = from 90% to 5% over 3 min. The method was performed with a flow rate of 1.0 mL/min. Compounds were only used for biological evaluation if the purity was ≥ 95%. ESI mass spectral data were acquired with a Shimadzu LCMS-2020. Data are reported as mass-to-charge ratio (m/z) of the corresponding positively charged molecular ions.

2,6-Difluoro-4-methylaniline (2). 1,3-difluoro-5-methyl-2-nitrobenzene **1** (1.0 g, 5.78 mmol) and 10% Pd-C (190 mg) in EtOH (20 mL) was hydrogenated under atmospheric pressure for 3 h. The catalyst was filtered off, and the filtrate was evaporated to give **2** as a light reddish oil (0.686 g, 4.80 mmol, 87%). ^{1}H-NMR ($CDCl_3$, 400 MHz): δ [ppm] = 6.63 (m, 2H), 3.49 (s, 2H), 2.23 (s, 3H). ^{13}C-NMR ($CDCl_3$, 400 MHz): δ [ppm] = 153.3 (d, *J* = 8.3 Hz), 151.0 (d, *J* = 8.3 Hz), 127.4 (t, *J* = 8.5 Hz), 121.1 (t, *J* = 16.6 Hz), 111.9 – 111.3 (m), 20.7 (t, *J* = 1.7 Hz). ESI-MS: *m/z* calc. for $C_7H_8F_4N_2^+$ $[M+H]^+$: 144.1, found: 144.1.

1-(2,6-Difluoro-4-methylphenyl)-2-(2,6-difluorophenyl)diazene (5). 2,6-Difluoraniline **3** (641 mg, 4.96 mmol, 2.00 equiv.) was dissolved in DCM (30 mL). To this solution, Oxone® (16.8g, 27.3 mmol, 20.00 equiv.) dissolved in water (60 mL) was added. The solution was under argon at room temperature overnight. After separation of the layers, the aqueous layer was extracted with DCM twice. The combined organic layers were washed with 1N HCl, saturated sodium bicarbonate solution, water, brine, dried over $MgSO_4$ and evaporated to dryness. Afterwards toluene (10 mL) and 2,6-difluoro-4-metylaniline **2** (357 mg, 2.49 mmol, 1.00 equiv.) were added. A mixture of acetic acid (20 mL) and TFA (50 mL) was prepared and added to the solution. The resulting mixture was stirred at room temperature for 24h. Afterwards it was evaporated to dryness. Purification by column chromatography over silica gel (DCM:PE,1:4, silica gel) yielded the desired product **5** as a deep orange solid (292 mg, 1.09 mmol, 43%). ^{1}H-NMR ($CDCl_3$, 400 MHz): δ [ppm] = 7.40 – 7.29 (m, 1H), 7.05 (t, *J* = 8.6 Hz, 2H), 6.87 (d, *J* = 10.5 Hz, 2H), 2.41 (s, 3H). ESI-MS: *m/z* calc. for $C_{13}H_9BF_4N_2^+$ $[M+H]^+$: 269.1, found: 269.1.

(4-(Phenyldiazenyl)phenyl)methanol (7). Nitrosobenzene **4a** (1.28 g, 11.9 mmol, 3 equiv.) was dissolved in ethanol (10 mL). To this solution (4-aminophenyl)methanol **6** (491 mg, 4.00 mmol, 1 equiv.) and acetic acid (20 mL) were added. The reaction mixture was stirred for 4 h at room temperature. Subsequently, the reaction mixture was poured into 30 mL of ice-cold water and the precipitate was collected by filtration. Column chromatography (DCM:methanol = 50:1) provided compound **7** (659 mg, 2.99 mmol, 75%) as bright orange needles. ^{1}H NMR (400 MHz, DMSO-d_6): δ [ppm] = 7.88 (m, *J* = 6.9, 1.8 Hz, 4H), 7.65 – 7.50 (m, 5H), 5.40 (t, *J* = 5.7 Hz, 1H), 4.61 (d, *J* = 5.6 Hz, 2H). ^{13}C NMR (101 MHz, DMSO-d_6): δ [ppm] = 152.4, 151.3, 146.9, 131.8, 129.93, 127.6, 122.9, 62.9. ESI-MS: *m/z* calc. for $C_{13}H_{12}N_2O^+$ $[M+H]^+$: 213.1, found: 213.1.

1-(4-(Bromomethyl)phenyl)-2-phenyldiazene (8a). (4-(phenyldiazenyl)phenyl)methanol **7** (300 mg, 1.41 mmol, 1 equiv.) was dissolved in dry THF (15 mL) under argon atmosphere, tetrabromomethane (703 mg, 2.12 mmol, 1.5 equiv.) and triphenylphosphine (556 mg, 2.12 mmol, 1.5 equiv.) were added and the reaction mixture was stirred for 4 h. The reaction mixture was filtered and the filtrate was evaporated to dryness and purified by column chromatography (EA:Hex = 1:10) giving yield to compound **8a** as orange needles (232 mg, 0.84 mmol, 60%). ^{1}H NMR (400 MHz, DMSO-d_6): δ [ppm] = 7.89 (tt, *J* = 7.7, 2.0 Hz, 4H), 7.69 – 7.57 (m, 5H), 4.80 (s, 2H).^{13}C NMR (101 MHz, DMSO-d_6): δ [ppm] = 151.9, 151.5, 141.5, 131.7, 130.5, 129.5, 122.9, 122.6, 33.6. ESI-MS: *m/z* calc. for $C_{13}H_{11}BrN_2^+$ $[M+H]^+$: 275.0, 277.0, found: 274.9, 276.9.

1-(4-(Bromomethyl)-2,6-difluorophenyl)-2-(2,6-difluorophenyl)diazene (8b). To a solution of 1,2-bis(2,6-difluoro-4-methylphenyl)diazene **5** (250 mg, 0.93 mmol) in 20 mL of CCl_4 was added NBS (0.332 g, 1.86 mmol) and AIBN (11 mg, 0.076 mmol). The resultant solution was stirred overnight at 80 °C. After evaporation of the solvent, the product was purified by column chromatography over silica gel (DCM:PE,1:4, silica gel) yielding the desired product **8b** (163 mg, 0.47 mmol, 50%). ^{1}H-NMR ($CDCl_3$, 400 MHz): δ [ppm] = 7.38 (t, *J* = 8.5 Hz, 4H), 7.21 (d, *J* = 8.5 Hz, 11H), 7.13 – 7.03 (m, 14H), 6.87 (dt, *J* = 14.8, 7.3 Hz, 42H), 6.65 (d, *J* = 8.8 Hz, 4H), 4.44 (s, 6H), 4.33 (s, 19H), 2.41 (s, 2H), 2.29 (s, 6H). ESI-MS: *m/z* calc. for $C_{13}H_8BrF_4N_2^+$ $[M+H]^+$: 347.0, 349.0 found: 347.0, 349.0.

4-((4,5-Dihydroisoxazol-3-yl)oxy)-N,N-dimethyl-N-(4-(phenyldiazenyl)benzyl)but-2-yn-1-aminium (9a). 1-(4-(bromomethyl)phenyl)-2-phenyldiazene **8a** (100 mg, 0.36 mmol, 1 equiv.) and 4-((4,5-dihydroisoxazol-3-yl)oxy)-*N,N*-dimethylbut-2-yn-1-amine **16** (132 mg, 0.73 mmol, 2 equiv.) were dissolved in acetonitrile (10 mL) and stirred at room temperature for 12 h. Reaction was monitored by LC-MS. The precipitate was filtered off and the solvent was removed under reduced pressure. The crude product was purified by column chromatography (DCM:MA:NH_3 = 20:1:0.1) giving yield to compound **9a** as a dark red oil (54 mg, 0.14 mmol, 39%). ^{1}H NMR (400 MHz, $CDCl_3$): δ [ppm] = 7.99 – 7.86 (m, 6H), 7.56 – 7.46 (m, 3H), 5.24 (s, 2H), 4.88 (d, *J* = 7.9 Hz, 4H), 4.42 (t, *J* = 9.6 Hz, 2H), 3.53 – 3.40 (m, 6H), 3.02 (t, *J* = 9.6 Hz, 2H). ^{13}C NMR (101 MHz, $CDCl_3$): δ [ppm] = 166.9, 154.1, 152.6, 134.3, 131.9, 129.3, 129.0, 123.7, 123.3, 87.8, 75.9, 70.2, 66.2, 57.5, 54.8, 50.0, 33.1. ESI-MS: *m/z* calc. for $C_{22}H_{25}BrN_4O_2^+$ $[M+H]^+$: 377.2, found: 377.2.

***N*-(4-((2,6-Difluorophenyl)diazenyl)-3,5-difluorobenzyl)-4-((4,5-dihydroisoxazol-3-yl)oxy)-*N,N*-dimethylbut-2-yn-1-aminium bromide (9b).** 1-(4-(bromomethyl)-2,6-difluorophenyl)-2-(2,6-difluorophenyl)diazene **8b** (64 mg, 0.184 mmol) and 4-((4,5-dihydroisoxazol-3-yl)oxy)-N,N-dimethylbut-2-yn-1-amine (34 mg, 0.184 mmol, 1 equiv.) in ethyl acetate (10 mL) were charged in a sealed reaction vessel and stirred for 4 h. The precipitate is collected and washed several times with ethyl acetate to afford the desired product **9b** as a bright yellow powder (90 mg, 0.170 mmol, 92%). ^{1}H-NMR (MeOD, 400 MHz): δ [ppm] = 7.63 – 7.30 (m, 3H), 7.12 (dt, J = 17.0, 8.7 Hz, 2H), 4.97 (d, J = 14.5 Hz, 2H), 4.66 (d, J = 49.0 Hz, 2H), 4.48 – 4.28 (m, 4H), 3.21 (d, J = 30.4 Hz, 6H), 3.05 (dt, J = 15.1, 9.6 Hz, 2H). ^{13}C-NMR (MeOD, 400 MHz): δ [ppm] = 168.82,

154.23 (d, J = 5.1 Hz), 151.71 (d, J = 5.5 Hz), 132.40 (t, J = 9.7 Hz), 131.22 (d, J = 9.0 Hz), 118.4, 118.1, 113.5 (d, J = 19.1 Hz), 89.1, 76.7, 71.2, 66.0, 58.3, 55.3, 51.1, 33.6. ESI-MS: m/z calc. for $C_{22}H_{21}F_4N_4O_2^+$ $[M]^+$: 449.16, found: 449.05.

1-Methyl-4-nitrosobenzene (11). *p*-Toluidine **10** (2.00 g, 18.7 mmol) was dissolved in DCM (60 mL), a solution of Oxone® (11.5 g, 18.7 mmol) in water (60 mL) was added. The resulting biphasic mixture was stirred at room temperature for 30 min. The organic layer was separated, and the aqueous layer was extracted twice with DCM. The combined organic layers were washed with 1 M aqueous hydrochlorid acid, saturated sodium hydrogen carbonate, and brine, and dried over anhydrous sodium sulfate. The mixture **11** was concentrated to 10 – 15 ml volume, which is further used without purification.

4,4'-Dimethylazobenzene (13a). 1-Methyl-4-nitrososbenzene **11** and *p*-toluidine **10** (1.00 g, 9.33 mmol) were dissolved in glacial acetic acid (20 mL) and stirred overnight. The solution was diluted with water and extracted with ethyl acetate. The organic phase was washed four times with water and once with brine and dried over anhydrous sodium sulfate. The crude product was purified by flash chromatography (pentane/diethyl ether, 9:1) to obtain the desired product **13a** as an orange crystalline solid (695 mg, 3.31 mmol, 36 %). ^{1}H NMR (400 MHz, $CDCl_3$): δ [ppm] = 7.82 (d, J = 8.3 Hz, 4H), 7.31 (d, J = 8.6 Hz, 4H), 2.44 (s, 6H). ^{13}C NMR (101 MHz, $CDCl_3$): δ [ppm] = 151.0, 141.3, 129.9, 122.9, 21.6. ESI-MS: *m/z* calc. for $C_{14}H_{14}N_2^+$ $[M+H]^+$: 211.1, found: 211.0.

1,2-bis(2,6-difluoro-4-methylphenyl)diazene (13b). 2,6-difluoro-4-methylaniline **12** (397m g, 2.77 mmol) and a freshly ground mixture of potassium permanganate (1.17 g, 4.21 mmol) and iron(II)sulphate heptahydrate (1.17 g, 7.40 mmol) were dissolved in DCM (10 mL). The solution was refluxed overnight, filtered through celite, dried over anhydrous sodium sulphate, filtered, and concentrated under reduced pressure. The crude residue was purified by column chromatography (DCM/petrol ether 1:1) to give the desired product **13b** (110 mg, 0.39 mmol, 29%). 1H-NMR (CDCl3, 400 MHz): δ [ppm] = 6.86 (d, J = 10.3 Hz, 4H, arom. trans), 6.65 (d, J = 8.3 Hz, 0.39H, arom. cis), 2.40 (s,6 H,-CH3, trans), 2.29 (s, 0.62H, -CH3, cis). 13C-NMR (CDCl3, 400 MHz): δ [ppm] = 156.8 (d, J = 5.0 Hz), 154.3 (d, J = 5.2 Hz), 143.2 (t, J = 10.3 Hz), 113.2, 113.0, 21.7.

4,4'-Bis(bromomethyl)azobenzene (14a). To a solution of 4,4'-dimethylazobenzene **13a** (2.17 g, 10.3 mmol) in 20 mL of carbon tetrachloride (40 mL) was added *N*-bromo succinimide (4.22 g, 23.7 mmol) and azobisisobutyronitrile (127 mg, 0.77 mmol). The resultant solution was stirred overnight at 70 °C, then filtered, and washed with chloroform, water and dried under reduced pressure, which yielded **14a** as orange crystalline powder (2.88 g, 7.81 mmol, 76%). ^{1}H NMR (400 MHz, $CDCl_3$): δ [ppm] = 7.90 (d, *J* = 8.4 Hz, 4H), 7.54 (d, *J* = 8.5 Hz, 4H), 4.56 (s, 4H). ^{13}C NMR (101 MHz, $CDCl_3$): δ [ppm] = 152.3, 140.8, 129.9, 32.7. ESI-MS: *m/z* calc. for $C_{12}H_{13}Br_2N_2^+$ $[M+H]^+$: 368.9, found: 368.8.

1,2-bis(4-(bromomethyl)-2,6-difluorophenyl)diazene (14b). To a solution of 1,2-bis(2,6-difluoro-4-methylphenyl)diazene **13b** (226 mg, 0.801 mmol) in 17 mL of CCl4 was added NBS (0.356 g, 2.02 mmol) and AIBN (10 mg, 0.060 mmol). The resultant solution was stirred overnight at 80 °C. After evaporation of the solvent, the product was

recrystallized from methanol to afford the desired product **14b** as red needles (86 mg, 0.195 mmol, 24%). 1H-NMR (CDCl3, 400 MHz): δ [ppm] = 7.11 (d, J = 9.1 Hz, 4H), 4.43 (s,4H). 13C-NMR (CDCl3, 400 MHz): δ [ppm] = 160.9 (d, J = 7.6 Hz), 158.8 (d, J = 6.7 Hz), 150.4 (t, J = 6.7 Hz), 125.2 (t, J = 27.2 Hz), 114.0 (dd, J = 26.7, 3.7 Hz), 30.6 (t, J = 3.7 Hz). ESI-MS: m/z calc. for C14H9Br2F4N2+ [M]+: 440.9, found: 440.7.

4-((4,5-Dihydroisoxazol-3-yl)oxy)-*N*-(4-((4-(((4-((4,5-dihydroisoxazol-3-yl)oxy)but-2-yn-1-yl)dimethyl-l4-azaneyl)methyl)phenyl)diazenyl)benzyl)-*N,N*-dimethylbut-2-yn-1-aminium bromide (15a). 4,4'-Bis(bromomethyl)azobenzene **14a** (100 mg, 0.272 mmol) and 4-((4,5-dihydroisoxazol-3-yl)oxy)-N,N-dimethylbut-2-yn-1-amine **16** were dissolved in 30 mL ethyl acetate and stirred at 60°C for 16 h. The precipitate was filtered and washed with cold ethyl acetate to afford the desired product **15a** as a yellow powder (166 mg, 0.227 mmol, 83%). ^{1}H NMR (400 MHz, DMSO-d_6): δ [ppm] = 8.03 (d, J = 8.4 Hz, 1H), 7.83 (d, J = 8.4 Hz, 1H), 4.99 (s, 1H), 4.75 (s, 1H), 4.47 (s, 1H), 4.33 (t, J = 9.6 Hz, 1H), 3.13 (s, 3H), 3.05 (t, J = 9.6 Hz, 1H).^{13}C NMR (101 MHz, DMSO-d_6): δ [ppm] = 166.8, 152.8, 134.2, 131.1, 123.0, 86.8, 76.3, 69.6, 64.9, 57.3, 53.3, 49.5, 32.3. ESI-MS: m/z calc. for $C_{32}H_{40}N_6O_4^{2+}$ $[M]^{2+}$: 286.2, found: 286.1.

***N,N'*-((Diazene-1,2-diylbis(3,5-difluoro-4,1-phenylene))bis(methylene))bis(4-((4,5-dihydroisoxazol-3-yl)oxy)-*N,N*-dimethylbut-2-yn-1-aminium) bromide (15b).** 4-((4,5-dihydroisoxazol-3-yl)oxy)-*N,N*-dimethylbut-2-yn-1-amine **16** (24.5 mg, 0.134 mmol) in ethyl acetate (40 mL) was slowly added to a stirred solution of 1,2-bis(4-(bromomethyl)-2,6-difluorophenyl)diazene **14b** (118 mg, 0.269 mmol, 2 equiv.) in ethyl acetate (10 mL) at 60°C. The reaction mixture was stirred for 18 h. The reaction mixture was evaporated to dryness and purified by reverse phase column chromatography (acetonitrile/water) yielding the desired product **15b** as a bright orange powder (35 mg, 0.043 mmol, 32%). ^{1}H-NMR (MeOD, 400 MHz): δ [ppm] = 7.55 (dd, J = 60.3, 8.6 Hz, 4H), 5.03 (dd, J = 7.6, 6.1 Hz, 4H), 4.77 (d, J = 38.9 Hz, 4H), 4.51 (s, 2H), 4.44 (s, 2H), 3.29 (d, J = 24.8 Hz, 12H), 3.09 (dt, J = 19.3, 9.7 Hz, 4H). ^{13}C-NMR (MeOD, 400 MHz): δ [ppm] = 176.6, 169.90, 168.9 (d, J = 2.4 Hz), 119.0, 118.4, 89.1, 76.7 (d, J = 7.4 Hz), 71.2, 58.4, 55.4 (d, J = 11.4 Hz), 51.2, 33.7. ESI-MS: m/z calc. for $C_{32}H_{36}F_4N_6O_4^{2+}$ $[M]^{2+}$: 322.14, found: 322.25.

General procedure for the synthesis of the homobivalent quaternary iperoxo dimers 18a-d. To a solution of 2 equiv. of 4-((4,5-dihydroisoxazol-3-yl)oxy)-*N,N*-dimethylbut-2-yn-1-amine **16** in 10 mL acetonitrile, 1 equiv. of the corresponding bromoalkane **17**-C4, **17**-C6, **17**-C8, and **17**-C10 and a catalytic amount of KI/K_2CO_3 (1:1) were added. The reaction mixture was heated in the microwave (500 W, 70 °C) for 2-3 h. After cooling to room temperature, the surplus of KI/K_2CO_3 was filtered off and the solvent was evaporated to half of the volume. The solution was kept in the fridge overnight. The precipitate obtained was filtered, washed with Et_2O and dried *in vacuo*.

***N*1,*N*4-Bis(4-((4,5-dihydroisoxazol-3-yl)oxy)but-2-yn-1-yl)-*N*1,*N*1,*N*4,*N*4-tetramethylbutane-1,4-diaminium bromide (18a).** Light, yellow solid; yield 69%. ^{1}H NMR (400 MHz, DMSO-d_6): δ [ppm] = 2.73-2.77 (m, 4H), 3.03 (t, 4H, J =

9.6 Hz), 3.12 (s, 12H), 3.44-3.48 (m, 4H), 4.33 (t, 4H, J = 9.6 Hz), 4.53 (s, 4H), 4.95 (s, 4H). ^{13}C NMR (101 MHz, DMSO-d_6): δ [ppm] = 19.1, 32.2, 49.7, 53.6, 57.2, 62.2, 69.6, 76.0, 86.1, 166.7. ESI-MS: *m/z* calc. for $C_{22}H_{36}N_4O_4^{2+}$ $[M]^{2+}$: 210.1 Found: 210.1

***N*1,*N*6-Bis(4-((4,5-dihydroisoxazol-3-yl)oxy)but-2-yn-1-yl)-*N*1,*N*1,*N*6,*N*6-tetramethylhexane-1,6-diaminium bromide (18b).** Light, yellow solid; yield 49%.^{1}H NMR (400 MHz, DMSO-d_6): δ [ppm] = 1.32-1.37 (m, 4H), 1.69-1.78 (m, 4H), 3.03 (t, 4H, J = 9.6 Hz), 3.11 (s, 12H), 3.36-3.40 (m, 4H), 4.33 (t, 4H, J = 9.6 Hz), 4,50 (s, 4H), 4.94 (s, 4H). ^{13}C NMR (101 MHz, DMSO-d_6): δ [ppm] = 21.6, 25.1, 32.2, 49.7, 53.3, 57.1, 62.9, 69.5, 76.1, 85.9, 166.6. ESI-MS: *m/z* calc. for $C_{24}H_{40}N_4O_4^{2+}$ $[M]^{2+}$: 224.2 Found: 224.1.

***N*1,*N*8-Bis(4-((4,5-dihydroisoxazol-3-yl)oxy)but-2-yn-1-yl)-*N*1,*N*1,*N*8,*N*8-tetramethyloctane-1,8-diaminium bromide (18c).** Light, yellow solid; yield 15%.^{1}H NMR (400 MHz, DMSO-d_6): δ [ppm] = 1.29-1.32 (m, 8H), 1.64-1.72 (m, 4H), 3.02 (t, 4H, J = 9.6 Hz), 3.10 (s, 12H), 3.39-3.41 (m, 4H), 4.32 (t, 4H, J = 9.6 Hz), 4,51 (s, 4H), 4.93 (s, 4H). ^{13}C NMR (101 MHz, DMSO-d_6): δ [ppm] = 21.7, 25.5, 28.1, 32.2, 49.7, 53.2, 57.2, 63.0, 69.5, 76.1, 85.9, 166.7. ESI-MS: *m/z* calc. for $C_{26}H_{44}N_4O_4^{2+}$ $[M]^{2+}$: 238.2 Found: 238.1.

***N*1,*N*10-Bis(4-((4,5-dihydroisoxazol-3-yl)oxy)but-2-yn-1-yl)-*N*1,*N*1,*N*10,*N*10-tetramethyldecane-1,10-diaminium bromide (18d).** Light, yellow solid; yield 36%.^{1}H NMR (400 MHz, DMSO-d_6): δ [ppm] = 1.30 (s, 12H), 1.62-1.72 (m, 4H), 3.02 (t, 4H, J = 9.2 Hz), 3.09 (s, 12H), 3.36-3.38 (m, 4H), 4.32 (t, 4H, J = 9.2 Hz), 4,51 (s, 4H), 4.93 (s, 4H). ^{13}C NMR (101 MHz, DMSO-d_6): δ [ppm] = 21.7, 25.6, 28.3, 28.6, 32.2, 49.7, 53.2, 57.1, 63.0, 69.5, 76.1, 85.8, 166.6. ESI-MS: *m/z* calc. for $C_{28}H_{48}N_4O_4^{2+}$ $[M]^{2+}$: 252.2 Found: 252.2.

Photochemical characterization. UV/Vis spectra and experiments were recorded on a Varian Cary 50 Bio UV/Vis Spectrophotometer using Hellma (Type 100-QS) cuvettes (10 mm light path). Data were plotted using GraphPad Prism 5.0. For irradiation, high performance LEDs (Mouser Electronics Inc. or Hartenstein) were used as light source. A concentration of 50 μM was prepared for each compound and measured in its dark-adapted state. Next, the probe is illuminated with LEDs of different wavelengths (254, 365, 380, 400, 430, 500 nm and white light) while gradually increasing the irradiation time until no change in the spectrum was detectable. Stability measurements were performed irradiating the probe with the light source, which provided the highest photoconversion to the *cis*-isomer and kept in dark for at least 120 minutes. During this time the absorbance at λ_{max} was recorded every 5 minutes. Lastly, the probe is irradiated with the light source, which provided the highest photoconversion to the *trans*-isomer. Photostationary distributions were determined by HPLC analysis using a 50 μM probe in physiological buffer. Absorption was measured at the respective isosbestic point wavelengths. Analysis was carried out with GraphPad Prism software (GraphPad Software Inc., San Diego CA, www.graphpad.com).

Pharmacology. *Cell culture.* All experiments were performed with HEK 293T cells stably expressing the novel split luciferase receptor sensor. Cells were incubated at 37 °C with 5% CO_2 and cultivated in DMED with 4500 mg/l glucose, 10%

(v/v) FCS, 100 μg/mL penicillin, 100 μg/mL streptomycin sulfate and 2 mM L-glutamine and 600 μg/mL G-418. Every two to three days the cell lines were routinely passaged.

Split Luciferase complementation assay. The assay was performed as described previously,[24] except for the following modifications: A Berthold Mithras LB 940 plate reader was used to quantify the luminescence emitted by the cells, using white, flat bottomed nunc™ f96 microwell™ polystyrene plates.

Molecular Modeling. In brief, all receptor-ligand docking experiments reported in this study were carried out with the CCDCs software GOLD version 5.1.[30] The active M_1 receptor homology model used as protein was previously reported.[27] All residues of the extracellular domains and the receptor core region were defined as potential binding pocket. Default settings were chosen for receptor-ligand docking and GoldScore was used as primary scoring function. All obtained docking poses and receptor-ligand interactions were analyzed with LigandScout 4.2 using 3D-pharmacophores.[31]

Binding experiments. [^{3}H]Quinuclidinyl benzilate ([^{3}H]QNB), ethanol solution, was purchased from Amersham Biosciences (catalog number TRK 604, 42 Ci/mmol, 1 mCi/ml). The experiments were carried out in 10 mM Tris-HCl buffer, pH 7.0, containing 6 mM $MgCl_2$. Rat brain cortices were used as a source of muscarinic receptors in the assay. After cleaning the meninges with buffer-soaked filter paper, cortices were dissected, and white matter was carefully trimmed off. This tissue was homogenized in 40 mL buffer using a Potter homogenizer with a motor-driven Teflon pestle. The homogenate was centrifuged for 30 min at 50,000 X *g*, and the resulting pellet was homogenized and centrifuged again. After protein determination by the Bradford assay, the final pellet was re-suspended at 1 mg of protein/ml, transferred to 1.5-ml microcentrifuge tubes, and centrifuged once more. After discarding the supernatant, membrane pellets were kept at -80 °C until use.[23] The general procedure consists of the incubation of 20 μg membrane protein with 200 pM [^{3}H]QNB (200 pM), in a total volume of 2 mL and in the presence of varying concentrations of competing compounds. An excess (2 μM) of the unlabeled muscarinic antagonist atropine was used to define nonspecific binding. After 45 min at 25 ^{o}C to reach equilibrium the reaction mixtures were quickly filtered through glass fiber disks using a semi-automated Brandel harvester allowing the simultaneous filtration of 24 samples.[21] Filters were washed twice with 4 mL of ice-cold Tris-HCl buffer (10mM, pH 7.0), and counted for radioactivity. The final results were reported as % binding of [^{3}H]QNB in each condition. This analysis was carried out with GraphPad Prism software (GraphPad Software Inc., San Diego CA, www.graphpad.com).

ASSOCIATED CONTENT

Supporting Information.

UV/VIS spectra, NMR data, HPLC traces, molecular modelling, binding experiments.

Molecular formula strings.

This material is available free of charge via the Internet at http://pubs.acs.org.

Accession codes

PDB code for the crystal structure of the human M_2 receptor in complex with agonist iperoxo is 4MQS. This crystal structure was used for the generation of the homology model for computational studies of the human M_1 receptor in complex with compound **9a**, **9b**, **15a**, **15b**, and **18a-d**.

AUTHOR INFORMATION

Corresponding Author

*Email: michael.decker@uni-wuerzurg.de

Notes

The authors declare no competing financial interests

ACKNOWLEDGMENT

L.A. and T.L. were supported by the International Doctoral Program "Receptor Dynamics: Emerging Paradigms for Novel Drugs" funded within the framework of the Elite Network of Bavaria (ENB). We kindly thank Professor Klaus Mohr from the Institute of Pharmacy and Toxicology at Bonn University for fruitful discussions.

REFERENCES

(1) a) Lerch, M. M.; Hansen, M. J.; van Dam, G. M.; Szymanski, W.; Feringa, B. L. Emerging Targets in Photopharmacology. *Angew. Chem. Int. Ed.* **2016**, *55*, 10978-10999; b) Velema, W. A.; Szymanski, W.; Feringa, B. L. Photopharmacology: Beyond Proof of Principle. *J. Am. Chem. Soc.* **2014**, *136*, 2178-2191; c) Hüll, K.; Morstein, J.; Trauner, D. In Vivo Photopharmacology. *Chem. Rev.* **2018**, *118*, 10710-10747; d) Broichhagen, J.; Frank, J. A.; Trauner, D. A Roadmap to Success in Photopharmacology. *Acc. Chem. Res.* **2015**, *48*, 1947-1960.

(2) a) Pittolo, S.; Gómez-Santacana, X.; Eckelt, K.; Rovira, X.; Dalton, J.; Goudet, C.; Pin, J.-P.; Llobet, A.; Giraldo, J.; Llebaria, A.; Gorostiza, P. An Allosteric Modulator to Control Endogenous G protein-coupled Receptors with Light. *Nat. Chem. Biol.* **2014**, *10*, 813-815; b) Schönberger, M.; Trauner, D. A Photochromic Agonist for μ-Opioid Receptors. *Angew. Chem. Int. Ed.* **2014**, *53*, 3264-3267; c) Agnetta, L.; Kauk, M.; Canizal, M. C. A.; Messerer, R.; Holzgrabe, U.; Hoffmann, C.; Decker, M. A Photoswitchable Dualsteric Ligand Controlling Receptor Efficacy. *Angew. Chem. Int. Ed.* **2017**, *56*, 7282-7287; d) Bahamonde, M. I.; Taura, J.; Paoletta, S.; Gakh, A. A.; Chakraborty, S.; Hernando, J.; Fernández-Dueñas, V.; Jacobson, K. A.; Gorostiza, P.; Ciruela, F. Photomodulation of G Protein-Coupled Adenosine Receptors by a Novel Light-Switchable Ligand. *Bioconjug. Chem.* **2014**, *25*, 1847-1854; e) Broichhagen, J.; Johnston, N. R.; von Ohlen, Y.; Meyer-Berg, H.; Jones, B. J.; Bloom, S. R.; Rutter, G. A.; Trauner, D.; Hodson, D. J. Allosteric Optical Control of a Class B G-Protein-Coupled Receptor. *Angew. Chem. Int. Ed.* **2016**, *55*, 5865-5868; f) Hauwert, N. J.; Mocking, T. A. M.; Da

Costa Pereira, D.; Kooistra, A. J.; Wijnen, L. M.; Vreeker, G. C. M.; Verweij, E. W. E.; De Boer, A. H.; Smit, M. J.; De Graaf, C.; Vischer, H. F.; de Esch, I. J. P.; Wijtmans, M.; Leurs, R. Synthesis and Characterization of a Bidirectional Photoswitchable Antagonist Toolbox for Real-Time GPCR Photopharmacology. *J. Am. Chem. Soc.* **2018**, *140*, 4232-4243; g) Westphal, M. V.; Schafroth, M. A.; Sarott, R. C.; Imhof, M. A.; Bold, C. P.; Leippe, P.; Dhopeshwarkar, A.; Grandner, J. M.; Katritch, V.; Mackie, K.; Trauner, D.; Carreira, E. M.; Frank, J. A. Synthesis of Photoswitchable Δ9-Tetrahydrocannabinol Derivatives Enables Optical Control of Cannabinoid Receptor 1 Signaling. *J. Am. Chem. Soc.* **2017**, *139*, 18206-18212; h) Dolles, D.; Strasser, A.; Wittmann, H.-J.; Marinelli, O.; Nabissi, M.; Pertwee, R. G.; Decker, M. The First Photochromic Affinity Switch for the Human Cannabinoid Receptor 2. *Adv. Therap.* **2018**, *1*, 1700032.

(3) Lohse, M. J.; Hofmann, K. P. Spatial and Temporal Aspects of Signaling by G-Protein-Coupled Receptors. *Mol. Pharmacol.* **2015**, *88*, 572-578.

(4) Burger, W. A. C.; Sexton, P. M.; Christopoulos, A.; Thal, D. M. Toward an Understanding of the Structural Basis of Allostery in Muscarinic Acetylcholine Receptors. *J. Gen. Physiol.* **2018**, *150*, 1360-1372.

(5) a) Kruse, A. C.; Kobilka, B. K.; Gautam, D.; Sexton, P. M.; Christopoulos, A.; Wess, J. Muscarinic Acetylcholine Receptors: Novel Opportunities for Drug Development. *Nat. Rev. Drug Discov.* **2014**, *13*, 549-560; b) Svoboda, J.; Popelikova, A.; Stuchlik, A. Drugs Interfering with Muscarinic Acetylcholine Receptors and Their Effects on Place Navigation. *Front. Psychiatry* **2017**, *8*, Article 215; c) van Koppen, C. J.; Kaiser, B. Regulation of Muscarinic Acetylcholine Receptor Signaling. *Pharmacol. Ther.* **2003**, *98*, 197-220; d) Eglen, R. M. Muscarinic Receptor Subtypes in Neuronal and Non-neuronal Cholinergic Function. *Auton. Autacoid. Pharmacol.* **2006**, *26*, 219-233.

(6) Wess, J.; Eglen, R. M.; Gautam, D. Muscarinic Acetylcholine Receptors: Mutant Mice Provide New Insights for Drug Development. *Nat. Rev. Drug Discov.* **2007**, *6*, 721-733.

(7) Caulfield, M. P. Muscarinic Receptors—Characterization, Coupling and Function. *Pharmacol. Ther.* **1993**, *58*, 319-379.

(8) a) Antony, J.; Kellershohn, K.; Mohr-Andrä, M.; Kebig, A.; Prilla, S.; Muth, M.; Heller, E.; Disingrini, T.; Dallanoce, C.; Bertoni, S.; Schrobang, J.; Tränkle, C.; Kostenis, E.; Christopoulos, A.; Höltje, H. D.; Barocelli, E.; De Amici, M.; Holzgrabe, U.; Mohr, K. Dualsteric GPCR Targeting: A Novel Route to Binding and Signaling Pathway Selectivity. *FASEB J.* **2009**, *23*, 442-450; b) Disingrini, T.; Muth, M.; Dallanoce, C.; Barocelli, E.; Bertoni, S.; Kellershohn, K.; Mohr, K.; De Amici, M.; Holzgrabe, U. Design, Synthesis, and Action of Oxotremorine-Related Hybrid-Type Allosteric Modulators of Muscarinic Acetylcholine Receptors. *J. Med. Chem.* **2006**, *49*, 366-372.

(9) a) Beharry, A. A.; Sadovski, O.; Woolley, G. A. Azobenzene Photoswitching without Ultraviolet Light. *J. Am. Chem. Soc.* **2011**, *133*, 19684-19687; b) Samanta, S.; Beharry, A. A.; Sadovski, O.; McCormick, T. M.; Babalhavaeji, A.; Tropepe, V.; Woolley, G. A. Photoswitching Azo Compounds I*n Vivo* with Red Light. *J. Am. Chem. Soc.* **2013**, *135*, 9777-84.

(10) a) Bleger, D.; Hecht, S. Visible-Light-Activated Molecular Switches. *Angew. Chem. Int. Ed.* **2015**, *54*, 11338-11349; b) Bléger, D.; Schwarz, J.; Brouwer, A. M.; Hecht, S. *o*-Fluoroazobenzenes as Readily Synthesized Photoswitches Offering Nearly Quantitative Two-Way Isomerization with Visible Light. *J. Am. Chem. Soc.* **2012**, *134*, 20597-20600.

(11) Dong, M.; Babalhavaeji, A.; Samanta, S.; Beharry, A. A.; Woolley, G. A. Red-Shifting Azobenzene Photoswitches for in Vivo Use. *Acc. Chem. Res.* **2015**, *48*, 2662-2670.

(12) a) Rullo, A.; Reiner, A.; Reiter, A.; Trauner, D.; Isacoff, E. Y.; Woolley, G. A. Long Wavelength Optical Control of Glutamate Receptor Ion Channels Using a Tetra-ortho-substituted Azobenzene Derivative. *Chem. Commun. (Camb.)* **2014**, *50*, 14613-14615; b) Wegener, M.; Hansen, M. J.; Driessen, A. J. M.; Szymanski, W.; Feringa, B. L. Photocontrol of Antibacterial Activity: Shifting from UV to Red Light Activation. *J. Am. Chem. Soc.* **2017**, *139*, 17979-17986; c) Konrad, D. B.; Frank, J. A.; Trauner, D. Synthesis of Redshifted Azobenzene Photoswitches by Late-Stage Functionalization. *Chemistry* **2016**, *22*, 4364-4368.

(13) Shonberg, J.; Scammells, P. J.; Capuano, B. Design Strategies for Bivalent Ligands Targeting GPCRs. *ChemMedChem* **2011**, *6*, 963-974.

(14) a) Mohr, K.; Schmitz, J.; Schrage, R.; Tränkle, C.; Holzgrabe, U. Molecular Alliance-From Orthosteric and Allosteric Ligands to Dualsteric/Bitopic Agonists at G Protein Coupled Receptors. *Angew. Chem. Int. Ed.* **2013**, *52*, 508-516; b) Halazy, S. G Protein-coupled Receptors Bivalent Ligands and Drug Design. *Expert Opin. Ther. Pat.* **2005**, *9*, 431-446.

(15) Nimczick, M.; Pemp, D.; Darras, F. H.; Chen, X.; Heilmann, J.; Decker, M. Synthesis and Biological Evaluation of Bivalent Cannabinoid Receptor Ligands Based on hCB(2)R Selective Benzimidazoles Reveal Unexpected Intrinsic Properties. *Bioorg. Med. Chem.* **2014**, *22*, 3938-3946.

(16) Decker, M.; Si, Y. G.; Knapp, B. I.; Bidlack, J. M.; Neumeyer, J. L. Synthesis and Opioid receptor Binding Affinities of 2-substituted and 3-Aminomorphinans: Ligands for Mu, Kappa, and Delta Opioid Receptors. *J. Med. Chem.* **2010**, *53*, 402-418.

(17) Kühhorn, J.; Hübner, H.; Gmeiner, P. Bivalent Dopamine D2 Receptor Ligands: Synthesis and Binding Properties. *J. Med. Chem.* **2011**, *54*, 4896-4903.

(18) a) Piergentili, A.; Quaglia, W.; Tayebati, S. K.; Paparelli, F.; Malmusi, L.; Brasili, L. Synthesis and Muscarinic Receptors affinity of a Series of Antagonist Bivalent Ligands. *Farmaco* **1994**, *49*, 83-87; b) Messer, J. W. Bivalent Ligands for G Protein-Coupled Receptors. *Curr. Pharm. Des.* **2004**, *10*, 2015-2020.

(19) Kloeckner, J.; Schmitz, J.; Holzgrabe, U. Convergent, Short Synthesis of the Muscarinic Superagonist Iperoxo. *Tetrahedron Lett.* **2010**, *51*, 3470-3472.

(20) Knie, C.; Utecht, M.; Zhao, F.; Kulla, H.; Kovalenko, S.; Brouwer, A. M.; Saalfrank, P.; Hecht, S.; Bléger, D. Ortho-Fluoroazobenzenes: Visible Light Switches with Very Long-Lived *Z* Isomers. *Chem. - Eur. J.* **2014**, *20*, 16492-16501.

(21) Claro, E. Analyzing Ligand Depletion in a Saturation Equilibrium Binding Experiment. *Biochem. Mol. Biol. Educ.* **2006**, *34*, 428-431.

(22) a) Yamamura, H. I.; Snyder, S. H. Muscarinic Cholinergic Binding in Rat Brain. *Proc. Natl. Acad. Sci. U. S. A.* **1974**, *71*, 1725-1729; b) Yamamura, H. I.; Kuhar, M. J.; Snyder, S. H. In Vivo Identification of Muscarinic Cholinergic Receptor Binding in Rat brain. *Brain Res.* **1974**, *80*, 170-176.

(23) Salles, J.; Wallace, M. A.; Fain, J. N. Differential Effects of Alkylating Agents on the Multiple Muscarinic Receptor Subtypes Linked to Activation of Phospholipase C by Carbachol in Rat Brain Cortical Membranes. *J. Pharmacol. Exp. Ther.* **1993**, *264*, 521-529.

(24) Littmann, T.; Ozawa, T.; Hoffmann, C.; Buschauer, A.; Bernhardt, G. A Split Luciferase-based Probe for Quantitative Proximal Determination of Gαq Signalling in Live Cells. *Sci. Rep.* **2018**, *8*, Article 17179.

(25) Hattori, M.; Ozawa, T. Split Luciferase Complementation for Analysis of Intracellular Signaling. *Anal. Sci.* **2014**, *30*, 539-544.

(26) Chen, X.; Klöckner, J.; Holze, J.; Zimmermann, C.; Seemann, W. K.; Schrage, R.; Bock, A.; Mohr, K.; Tränkle, C.; Holzgrabe, U.; Decker, M. Rational Design of Partial Agonists for the Muscarinic M1 Acetylcholine Receptor. *J. Med. Chem.* **2015**, *58*, 560-576.

(27) Bermudez, M.; Rakers, C.; Wolber, G. Structural Characteristics of the Allosteric Binding Site Represent a Key to Subtype Selective Modulators of Muscarinic Acetylcholine Receptors. *Mol. Inform.* **2015**, *34*, 526-530.

(28) a) Bock, A.; Bermudez, M.; Krebs, F.; Matera, C.; Chirinda, B.; Sydow, D.; Dallanoce, C.; Holzgrabe, U.; De Amici, M.; Lohse, M. J.; Wolber, G.; Mohr, K. Ligand Binding Ensembles Determine Graded Agonist Efficacies at a G Protein-coupled Receptor. *J. Biol. Chem.* **2016**, *291*, 16375-16389; b) Bermudez, M.; Bock, A.; Krebs, F.; Holzgrabe, U.; Mohr, K.; Lohse, M. J.; Wolber, G. Ligand-Specific Restriction of Extracellular Conformational Dynamics Constrains Signaling of the M2 Muscarinic Receptor. *ACS Chem. Biol.* **2017**, *12*, 1743-1748.

(29) Dror, R. O.; Green, H. F.; Valant, C.; Borhani, D. W.; Valcourt, J. R.; Pan, A. C.; Arlow, D. H.; Canals, M.; Lane, J. R.; Rahmani, R.; Baell, J. B.; Sexton, P. M.; Christopoulos, A.; Shaw, D. E. Structural Basis for Modulation of a G-Protein-coupled Receptor by Allosteric Drugs. *Nature* **2013**, *503*, 295-299.

(30) Jones, G.; Willett, P.; Glen, R. C.; Leach, A. R.; Taylor, R. Development and Validation of a Genetic Algorithm for Flexible Docking. *J. Mol. Biol.* **1997**, *267*, 727-748.

(31) Wolber, G.; Seidel, T.; Bendix, F.; Langer, T. Molecule-pharmacophore Superpositioning and Pattern Matching in Computational Drug Design. *Drug Discov. Today* **2008**, *13*, 23-29.

Table of Content Graphic: